Fe-N-doped Carbon Capsules with Outstanding Electrochemical Performance and Stability for the Oxygen Reduction Reaction in Both Acid and Alkaline Conditions

Guillermo A. Ferrero,[a] Kathrin Preuss,[b] Adam Marinovic,[b] Ana Belen Jorge,[c,d] Noramalina Mansor,[e] Dan J. L. Brett,[e] Antonio B. Fuertes,[a] Marta Sevilla,[a,*] Maria-Magdalena Titirici[b,*]

[a] Instituto Nacional del Carbón (CSIC), P.O. Box 73, Oviedo 33080, Spain

[b] School of Engineering and Materials Science, Queen Mary University of London, Mile End Road, E1 4NS, London, UK

[c] Department of Chemistry, University College London, WC1H 0AJ, London, UK

[d] Materials Research Institute, School of Engineering and Materials, Queen Mary University of London, E1 4NS, London, UK

[e] Department of Chemical Engineering, University College London, London WC1E 7JE, UK

* Corresponding authors:mailto:martasev@incar.csic.es martasev@incar.csic.es (M. Sevilla),

m.m.titirici@qmul.ac.uk (M.-M. Titirici)

Abstract

High surface area N-doped mesoporous carbon capsules with iron traces exhibit outstanding electrocatalytic activity for the oxygen reduction reaction (ORR) in both alkaline and acidic media. In alkaline conditions, they exhibit a more positive onset (0.94 V *vs.* RHE) and half-wave potentials (0.83 V *vs.* RHE) than commercial Pt/C, while in acidic media the onset potential is comparable to

that of commercial Pt/C with a peroxide yield lower than 10 %. The Fe-N-doped carbon catalyst combines the high catalytic activity with remarkable performance stability (3500 cycles between 0.6 and 1.0 V *vs.* RHE), which stems from the fact that iron is coordinated to nitrogen. Additionally, the newly developed electrocatalyst is unaffected by the methanol cross-over effect in both acid and basic media, contrary to commercial Pt/C. The excellent catalytic behavior of the Fe-N-doped carbon, even in the more relevant acid medium, is attributable to the combination of chemical functions (N-pyridinic, N-quaternary and Fe-N coordination sites) and structural properties (large surface area, open mesoporous structure and short diffusion paths), which guarantees a large number of highly active and fully accessible catalytic sites and rapid mass-transfer kinetics. Thereby, this catalyst represents an important step forward towards replacing Pt catalysts with cheaper alternatives. In this regard, an alkaline anion exchange membrane fuel cell was assembled with the Fe-N-doped mesoporous carbon capsules as the cathode catalyst providing current and power densities matching those of a commercial Pt/C, which glimpses the practical applicability of the Fe-N-carbon catalyst.

Keywords: carbon nanomaterial, nitrogen-doping, oxygen reduction reaction, non-noble metal catalysts, capsule

One major limitation in the performance of proton exchange membrane (PEM) fuel cells is the sluggish kinetics of the oxygen reduction reaction (ORR) occurring at the cathode.[1, 2] This issue compromises their widespread utilization and commercialization. Traditionally, platinum has been considered as the best catalyst for the ORR, taking into account its high activity *via* four electrons transfer leading to water as the final product. However, platinum is scarce, its performance degrades in time and it is very expensive.[3, 4] Considerable research efforts have been directed towards the discovery of cost-effective materials exhibiting comparable catalytic performance to platinum, while showing a better tolerance towards CO poisoning. The development of non-precious metal catalysts [5-8] and metal-free catalysts [9] has gained increasing research attention due to their good catalytic activity towards ORR, low cost and good durability. Despite exhaustive research in non-precious metal and metal-free ORR catalysts, the challenge remains to be able to maintain or even increase the electrochemical performance and durability at the PEMFC's cathode.[10, 11]

Heteroatom-doped carbon materials are promising alternatives as ORR catalysts -often *via* a $4e^-$ route similar to platinum-, with high current densities and high onset potential.[12] Among various dopants, nitrogen has been extensively studied due to its enhanced electrocatalytic activity for ORR, in addition to other beneficial properties, such as increased electrical conductivity and oxidation stability. [13-16] ENREF_12 The main drawback of N-doped metal-free carbon materials when used as electrocatalysts is their poor performance and poor stability in acidic media.[2, 17-20] Indeed, most reports show excellent N-

doped electrocatalysts in alkaline media,[21-25] but only very few groups have shown a good performance in acid media.[26-29] Furthermore, even if previously reported N-doped metal-free carbons exhibited a good performance in acid media, their performance drastically decreased after several cycles due to the degradation of the carbon matrix.[2, 12, 24] To overcome these difficulties, N-doping has been combined with the addition of non-precious metals such as cobalt or iron, leading to catalysts that exhibit a higher activity, long-term stability and better tolerance to poisons than only N-doped carbons.[27, 30, 31] Within this context, one of the most promising catalysts is a carbon material containing Fe–N moieties on the surface (Fe–N–C) which, even with only iron traces, shows a higher catalytic activity.[11, 32-34] _ENREF_11 The main active site is believed to be iron coordinated to nitrogen, which has been demonstrated to play a major role in the ORR process. [11, 35]

Herein, we report on N-doped mesoporous carbon capsules with iron traces as ORR electrocatalyst with remarkable performance and stability under both acid and alkaline conditions. This material was synthesized by using pyrrole as carbon precursor and non-porous core/mesoporous shell silica particles as sacrificial template. The use of $FeCl_3$ for the oxidative polymerization of pyrrole leads to a N-doped carbon material with traces of iron, which cannot be dissolved even after harsh acid treatment as a consequence of the fact that part of it is coordinated to nitrogen and the other is as Fe_3C encapsulated in a relatively thick graphitic layer (~ 15 nm). Although the use of pyrrole as carbon precursor for ORR catalysts has already been reported,[36-38] the electrocatalytic activity of such catalysts in acid electrolyte is far from that of commercial platinum. However, our ORR electrocatalysts exhibit several properties that are

highly important for an effective performance: a) a large number of nitrogen functional groups within the carbon framework due to the use of pyrrole as the carbon precursor; b) the presence of nitrogen-iron coordination sites; c) a high specific surface area (~ 1600 m^2 g^{-1}) and a porosity made up of uniform mesopores (~ 3.8 nm) due to the mesoporous shell of the silica template; d) a hollow morphology that entails a uniform thin carbon layer (thickness ~ 50 nm) greatly reducing diffusion distances and e) the existence of graphitic domains enhancing their electronic conductivity. The combination of all these chemical and structural properties guarantees a large number of highly active and fully accesible catalytic sites and rapid mass-transfer kinetics. Consequently, our electrocatalyst exhibits a high ORR activity - which is close to or higher than that of the Pt/C catalyst - in both basic and acid media. It is worth noting that the excellent electrocatalytic activity has been confirmed by using a rotating ring-disk electrode, which has allowed assessing the reaction mechanism and quantifying the percentage of harmful H_2O_2 produced, a procedure not widely used in the literature.[19, 21-23] Furthermore, an alkaline fuel cell (AAEMFC) has been succesfully assembled with the Fe-N-doped cathode catalyst.

Results and discussion

Structural and chemical properties of the N-doped carbon capsules

An illustration of the synthetic method is shown in Figure 1. In order to synthesize porous hollow carbon particles, we used as template silica particles with a structure formed by a solid core and a mesoporous shell, and pyrrole as carbon precursor and N-dopant. The pores of the silica particles were impregnated with $FeCl_3$ and, then, infiltrated with pyrrole vapors which rapidly

polymerized to polypyrrole. Subsequently, the silica-polypyrrole composite was carbonized and the silica framework and most of iron were dissolved with hydrofluoric acid, giving rise to Fe-N-doped carbon capsules (Fe-N-CC).

The SEM image in Figure 2a shows that the carbon particles have a spherical morphology with a uniform diameter of 580 ± 40 nm (see inset in Figure 2a). These microspheres exhibit a hollow structure, as evidenced by the high-magnification TEM image displayed in Figure 2b, which reveals that the diameter of the central macroporous core is around 330 ± 40 nm with a porous shell of around 50 nm thick. These carbon particles exhibit a high BET (Brunauer–Emmett–Teller) surface area of 1590 m^2 g^{-1} and a large pore volume of 1.46 cm^3 g^{-1} (see Table 1). Importantly, the porosity of the carbon layer is made up almost exclusively of mesopores, as calculated by means of the α_s-plot method applied to the N_2 adsorption branch (see inset in Figure 2c), with the micropores representing only < 5 % of the total pore volume (Table 1). These mesopores have a uniform size centered at around 3.8 nm, as deduced by the Kruk-Jaroniec-Sayari (KJS) method applied to the N_2 isotherm adsorption branch (Figure S1).

The microstructure of the Fe-N-CC sample was investigated by X-ray diffraction (XRD). A sharp peak can be observed at 2θ = 26°, which corresponds to the (*002*) diffraction peak of graphite (see Figure S2a). This peak is superimposed on a broad profile corresponding to amorphous carbon, suggesting the presence of a certain amount of graphitized carbon embedded in an amorphous carbon matrix. The presence of these graphitic domains is attributable to the iron nanoparticles generated during the high temperature treatment (derived from the $FeCl_3$ used for the oxidative polymerization of

pyrrole), which act as a graphitization catalyst during the carbonization, converting a certain amount of amorphous carbon into graphitic nanostructures.[39-41] No peaks attributable to Fe/Fe_3C nanoparticles can be observed, whereas the XRD pattern of the sample before the harsh acid washing showed the presence of a small amount of metal Fe and Fe_3C (see Figure S2b). The existence of the graphitic domains was further confirmed by Raman spectroscopy performed in randomly selected regions. Thus, as can be seen in Figure S2c, the Raman spectrum corresponding to an amorphous carbon region is composed of two broad overlapping D and G bands (I_D/I_G = 1.14, FWHM of G band = 68 cm^{-1}), whereas that of the graphitic carbon regions exhibits a high-intensity sharp G band at 1575 cm^{-1} and a weak D band at 1350 cm^{-1} (I_D/I_G = 1.2, FWHM of G band = 37 cm^{-1}) associated to defects in the graphitic sp^2 carbon structures. The amount of graphitic carbon in the Fe-N-CC sample is around 10 wt %, as deduced by means of thermogravimetric analysis (see Figure S2d). The electrical conductivity of the Fe-N-CC sample is 22 S m^{-1} (see Table 1). This good value of conductivity can be attributed to the combination of N-doping and the presence of a certain amount of graphitic domains.

The bulk nitrogen content of the Fe-N-CC sample -as determined by elemental analysis- is 5.88 wt % (Table 1). The analysis of the chemical nature of the nitrogen groups inserted within the carbon framework was performed through X-ray photoelectron spectroscopy (XPS) (Figure 2d). The high-resolution N 1s XPS spectrum can be deconvoluted in two main peaks at 398.6 and 400.9 eV, which are assigned respectively to pyridinic-N (N-6; 40.4%) and quaternary-N (N-Q; 53.7%), and a minor peak at 402.7 eV, which can be

attributed to pyridine-N-oxides (N-O; 5.9 %).[42, 43] The N/C atomic ratios corresponding to the bulk -elemental analysis- (0.064) and the surface -XPS analysis- (0.068) (see Figure S3a) of the particles are similar, indicating that the nitrogen functionalities are homogeneously distributed throughout the particles. The XPS general spectrum in Figure S3a further evidences the presence of a small amount of Fe (~710 eV). Specifically, 0.2 at % Fe remains after four days of harsh acid washing with HF (48 %) which reveals the high chemical stability of the Fe-N-doped carbon capsules. ICP analysis also shows a bulk iron content of 0.2 at % (~ 0.7 wt %). Deconvolution of the high-resolution Fe $2p_{3/2}$ XPS spectrum (Figure S3b) hints at the presence of iron coordinated to nitrogen, but no Fe_3C can be detected (see further discussion in SI), both of which have been shown to be active in ORR. [44, 45] However, taking into account that only traces of iron are present, it is hard to accurately analyze the iron species by XPS (detection limit ~ 0.1-0.2 at %). Therefore, in order to get more insights into the kind of iron species present in the material, TEM/HRTEM studies were performed. The EDX-TEM mapping images in Figure S4 show that C, N, O and Fe in the Fe-N-CC sample are homogenously distributed. It must be noted that no nanoparticles containing iron species are observable in the capsules in the TEM picture in Figure S4a, but EDX shows that this element is homogeneous distributed within the carbon framework. Further analysis was therefore performed by calculating the EDX concentration profiles of N and Fe along the line drawn on these carbon capsules (see Figure 3a). As can be seen in Figure 3b, the iron and nitrogen profiles perfectly correlate with each other, suggesting that the iron atoms are coordinated to nitrogen (Fe-N_x). However, this is not the only iron species found by HRTEM. As revealed by Figure S5a,

Fe_3C nanoparticles are found encapsulated by a graphitic layer. A closer look at these nanoparticles reveals that they are coated by a graphitic carbon layer of around 15 nm (see Figure S5b), with an interlayer spacing of 0.336 nm, corresponding to the (002) plane of graphitic carbon. As shown in Figures S5c and S5d for a typical nanoparticle, the spacing of the crystalline lattices in two directions was 0.236 nm and 0.200 nm, which are incompatible with the iron phases, but can be assigned to Fe_3C phase. It should be noted that the Fe_3C particles constitute a minor amount as deduced by TEM inspection. The presence of a graphitic layer surrounding Fe_3C explains why those particles are not detected by XPS, whose analysis depth is < 10 nm, and also why they are not removed after acid washing. It must be pointed out that, in order to test the reproducibility of this procedure, the synthesis was repeated several times. In all the cases, the chemical and the textural properties of the Fe-N-doped carbon capsules were similar.

Electrocatalytic performance of the N-doped carbon capsules in the oxygen reduction reaction (ORR)

The electrocatalytic activity of the Fe-N-doped carbon capsules towards ORR was assessed in both acidic and alkaline electrolytes. The ORR activity was first studied in a three-electrode cell configuration by using cyclic voltammetry in N_2- and O_2-saturated 0.1 M KOH and 0.5 M H_2SO_4 solutions. Figures S6a and S6b show the CV curves of Fe-N-CC in N_2- and O_2-saturated electrolytes at a scan rate of 100 mV s^{-1}. In both cases, featureless voltammetric curves are observed in the N_2-saturated solution. The voltammograms only exhibit capacitive charging currents associated with the

surface area of the particles and pseudocapacitive currents attributable to the N- and O- groups.[46] In contrast, when the electrolyte is saturated with O_2, a well-defined cathodic peak is observed at around 0.82 V in KOH (see Figure S6a) and 0.58 V in H_2SO_4 (see Figure S6b), which suggests pronounced ORR electrocatalytic activity. The value of peak potential obtained in basic medium is shifted to positive values when compared to some of the top-performing N-doped carbon materials that can be found in the literature. [22, 47-51] These results highlight the outstanding electrocatalytic performance of Fe-N-CC, which may be attributable to a synergetic effect between N- and Fe-doping. Taking into account that carbon materials are less active in acid than in alkaline medium,[2] the pronounced cathodic peak found in 0.1 M KOH is less sharp in 0.5 M H_2SO_4. Nevertheless, it is still noticeable compared to other catalysts that can be found in the literature,[52-54] ENREF_41 which suggests also good catalytic activity in acid medium.

A detailed investigation of the mass-transfer kinetics and electrochemical performance of the Fe-N-CC sample was carried out by experiments performed using a rotating disk electrode (RDE) and a rotating ring-disk electrode (RRDE). The polarization curves obtained from RDE (1600 rpm) linear sweep voltammetry in O_2-saturated 0.5 M H_2SO_4 and 0.1 M KOH are shown in Figures 4a and 4b, respectively. To provide a realistic picture, the results are compared with those of a commercial Pt/C catalyst (20 wt % Pt) using the same amount of each catalyst (0.1 mg cm^{-2}). In 0.1 M KOH, the ORR polarization curve of Fe-N-CC exhibits a high onset (*ca*. 0.94 V) and half-wave potentials (*ca.* 0.83 V), both values being higher than those of Pt/C (*ca*. 0.93 V and *ca*. 0.78 V respectively). A comparison of the value of onset potential of Fe-N-CC with that of state-of-

the-art N-doped and Fe-N-doped carbon materials evidences the outstanding activity offered by Fe-N-CC in basic medium (see Table S1). On the other hand, in 0.5 M H_2SO_4, the Fe-N-CC sample possesses a similar onset potential (0.80 V) to that of Pt/C (*ca*. 0.80 V, comparable to that found by other authors for analogous mass loading[36, 55]), although the half-wave potential is slightly decreased (*ca*. 0.52 V *vs.* 0.60 for Pt/C).[36] This value of onset potential is comparable to the best N- and Fe-N-doped carbon catalysts reported so far in the literature (see Table S2). Especially remarkable is the behavior in basic medium in which the diffusion-limited current density is significantly improved (by 10 %) in relation to Pt/C (Note that the mass loadings of both catalyst are the same, 0.1 mg cm^{-2}) and superior to many advanced N-doped and Fe-N doped carbon catalysts reported in the literature.[48, 56-58] It is worth noting that the value of diffusion-limited current density measured for commercial Pt/C is in agreement with other reported values for the same mass loading of catalyst.[22, 23, 47, 59]

The ORR kinetics in acidic and alkaline media was also assessed by using the Koutecky-Levich equation. The rotation dependent currents in Figures S7a-S7b show a linear reciprocal square-root relationship according to the Koutecky-Levich plot (see Figure S7c-S7d), with a slope more similar to an ideal four-electron process than to an ideal two-electron process. More specifically, in 0.1 M KOH, the number of electrons thus calculated is 3.7 at 0.58 V (see Figure S7c). This result suggests that Fe-N-CC catalyzes the direct four-electron oxygen reduction reaction to OH^-. The calculated electrochemical kinetic current density (J_K) value of 18.3 mA cm^{-2} at 0.58 V is more than three times higher than that of commercially available Pt/C (5 mA cm^{-2} at 0.58 V,

value similar to those reported in the literature for the same mass loading of Pt/C[47, 59]) in basic medium. Furthermore, this value is superior to that of many nitrogen and Fe-N doped carbons found in the literature (see Table S1). In acidic medium, Fe-N-CC also catalyzes the four-electron process (see Figure S7d) with a J_K value of 4.85 mA cm^{-2} at 0.46 V, still superior to commercial Pt/C (4 mA cm^{-2}, value again comparable to the literature[60]). These results reveal the high electrocatalytic activity towards ORR compared to Pt/C.

A more in-depth study of the reaction pathway was performed with a RRDE, in which the amount of HO_2^- can be accurately determined. Figures 4c-4d provide a comparison of the number of electrons transferred along with the yield of peroxide formed for the Fe-N-CC carbon capsules and Pt/C in 0.1 M KOH and 0.5 M H_2SO_4 electrolytes. The Fe-N-CC sample shows an *n* value higher than 3.8 in basic medium and the HO_2^- formation is lower than 10 % over the whole range of potentials, demonstrating its excellent electrocatalytic selectivity. In acidic medium, the H_2O_2 yield is even lower, *i.e.* < 8 %, while the number of electrons transferred is kept at ~ 3.8 (see Figure 4d). These results clearly indicate that ORR on Fe-N-CC carbon proceeds *via* the efficient four-electron pathway.[61] This is very important from an operation point of view, as the H_2O_2 produced on the two-electron process may degrade the catalyst layer and the membrane.[62]

With the aim of assessing the role of iron on creating ORR catalytic active sites, we investigated the ORR activity of Fe-N-CC in 0.1 M KOH containing 10 mM KCN. It is well known that CN^- ions can coordinate strongly to iron and, therefore, poison the iron-centered catalytic sites for ORR,[63] whereas the nitrogen active centers are inert to CN^- ions.[64] As can be seen in Figure 5, the

addition of KCN negatively shifts the onset and half-wave potentials respectively by ~ 57 and ~ 60 mV. In addition, a 16 % decrease is recorded on the diffusion limited current. These results show that part of the activity of the Fe-N-doped carbon capsules is indeed attributable to the Fe-N coordination sites identified in the capsules (*vide supra*). Contribution of the Fe_3C phase can be discarded taking into account that it is encapsulated in a graphitic carbon layer which does not allow penetration of the electrolyte. Anyway, Figure 5 also proves that the catalytic activity of the N-sites is not negligible at all. In fact, the Fe-N-carbon catalyst poisoned with CN^- exhibits a limiting current density which is just ~ 8 % lower than that of commercial Pt/C and an onset potential of 0.89 V. Furthermore, these values are still higher or comparable to those of many top-performing metal-free N-doped carbons. [48, 54, 59, 65, 66] ENREF_58 ENREF_64 ENREF_47 ENREF_65 Indeed, the carbon particles contain a great number of active sites (N-groups) that are well-distributed along a large surface area, thereby providing numerous catalytic centers for O_2 chemisorption and reduction.[67, 68] Importantly, most of the N-groups correspond to quaternary and pyridinic nitrogen, which are the two main contributors to the electrocatalytic activity.[13, 69] Summarizing, the above results clearly show that there are two types of active sites coexisting in the Fe-N-carbon capsules catalysts, *i.e.* Fe-N and N. Besides, the carbon particles exhibit an optimized pore structure made up of uniform mesopores of *ca.* 4 nm and short diffusional paths arising from an effective particle size ~ 50 nm, which ensure fast mass-transfer processes and maximize exposure of the nitrogen and iron active sites to the reactants/electrolyte enhancing their utilization.[70]

The long-term stability of ORR catalysts is also a major concern in fuel-cell technology and, therefore, much attention has been paid recently to this feature.[6] Accordingly, the durability of the Fe-N-CC catalyst was tested following a US Department of Energy's accelerated durability test protocol based on cycling the catalysts between 0.6 and 1.0 V (*vs.* RHE) at 50 mV s^{-1} under N_2 atmosphere in 0.1 M KOH and 0.5 M H_2SO_4.[27, 31] Figures 6a-6b compare the linear sweep voltammetry curves at a rotation speed of 1600 rpm in O_2-saturated electrolyte before and after the accelerated durability test in KOH and H_2SO_4 electrolytes. In KOH, the Fe-N-CC catalyst exhibits a remarkable durability performance, in which the onset potential decreases by only ~20 mV after 3500 cycles, with no appreciable variation in the half-wave potential. On the contrary, commercial Pt/C exhibits a decrease of the onset and half-wave potentials of 10 and 90 mV respectively. Chronoamperometric testing was carried out to confirm the durability of the nitrogen-doped carbon capsules and commercial Pt/C in 0.1 M KOH. The results shown in Figure S8 reveal that the Fe-N-CC sample retains *ca.* 90 % of the initial current after 10,000 s, whereas commercial Pt/C retains only 70 % of the initial current. In H_2SO_4, after 3500 continuous cycles, the half-wave potential of Fe-N-CC shows a negative shift of ~40 mV and the onset potential slightly decreases from 0.80 V to 0.76 V (see Figure 6b). These values show improved resistance to performance decay when compared to Pt/C, which suffers a decrease of 70 mV on the onset potential and 140 mV on the half-wave potential. These results prove the robustness of the Fe-N and N catalytic sites regardless of the electrolyte used, which was already suggested by their resistance to the harsh acid washing.

One of the disadvantages of platinum-based electrocatalysts in direct methanol fuel cells (DMFC), is methanol crossover from the anode to the cathode.[71] To analyze this issue, the chronoamperometric response was measured by injecting methanol into the O_2-saturated 0.1 M KOH electrolyte (see Figure 6c). Both Fe-N-CC and Pt/C catalysts show ORR activity when oxygen is bubbling. However, after the injection of methanol (t = 160 s), a dramatic loss of cathodic current is registered in the platinum catalyst, indicating rapid degradation of its ORR activity.[25, 72] In contrast, Fe-N-CC catalyst does not show any sensitivity towards the presence of methanol, the cathodic current remaining relatively stable after methanol injection. Similar results were obtained in acid medium. Thus, Fe-N-CC electrocatalyst shows excellent tolerance to methanol crossover with an equally good ORR performance with or without methanol (see Figure 6d). These results clearly show that the Fe-N-doped carbon particles constitute an outstanding catalyst in the ORR process regardless of the type of electrolyte or fuel used.

Alkaline anion exchange membrane fuel cell (AAEMFC) assembly

The real applicability of the Fe-N-CC catalyst was assessed by using with Fe-N-CC and Pt/C as cathode catalysts in AAEMFC. The polarization curves in Figure 7 show that commercial Pt/C performs better than Fe-N-CC at low current density (< 100 mA cm^{-2}), but worse at high current density. However, overall, Fe-N-CC produces a higher power density than Pt/C. EIS analysis was carried out to determine the exact contribution of the catalyst with respect to other factors, such as Ohmic resistance and mass transport, to the overall performance of the cell. Half-cell impedance spectra of the anode and cathode, in addition to the whole cell, were also measured. Figure S9 shows the Nyquist

plots corresponding to the cathode and the whole cell measurements at various current densities. The contribution from the anode is insignificant in all cases, especially at low current density. Therefore, it can be assumed that cathode kinetics are the dominant factor affecting the overall performance. Regardless of the current density, the charge transfer resistance of Fe-N-CC is significantly lower than that of Pt/C, which confirms the RDE results. However, the low charge transfer resistance shown by the EIS measurements is not reflected in an improved performance in the polarization curve at low current densities as shown by Figure 7. This is mainly due to the lower starting potential (0.96 V *vs*. 1.01 V) of the Fe-N-CC fuel cell at open circuit voltage (OCV). The low OCV could be caused by other reasons such as mixed potential or gas crossover.[62, 73] However, as more current is drawn from the fuel cell, the improved performance expected from the EIS and RDE measurements manifests itself in lower voltage losses compared to Pt/C. These results suggest that Fe-N-CC could serve as a good substitute for Pt/C as cathode catalyst. Improvements in the CCM fabrication method would further enhance the fuel cell performance.

Conclusions

In summary, a novel ORR iron and nitrogen doped hollow carbon electrocatalyst has been synthesized using the nanocasting approach and pyrrole as N-rich carbon precursor. The resulting carbon particles possess iron traces mainly in the form of Fe-N coordination sites (~ 0.7 wt %) and a high content of nitrogen moieties (~ 6 wt %) comprising mainly quaternary and pyridinic groups. The structure of these hollow particles consists of a highly porous (S_{BET} ~ 1500 m^2 g^{-1}), curved, thin carbon layer (thickness ~ 50 nm)

containing pores with a size centered at around 4 nm. This remarkable combination of chemical and structural properties gives rise to an active ORR electrocatalyst with numerous and easily accessible catalytic centers. Importantly, it has been shown that both N-sites and Fe-N coordination sites are contributing to the catalytic activity. Thereby, the Fe-N-doped hollow carbon particles exhibit an outstanding activity in basic media and an excellent (comparable to Pt/C) performance in acidic media, with a peroxide yield lower than 10 %, an electron transfer number close to 4, and onset and half-wave potentials superior (basic media) or similar (acid media) to those of commercial Pt/C. Furthermore, these nitrogen-doped carbon capsules with iron traces exhibit an excellent resistance to methanol crossover and a superior long-term durability, beating the platinum supported carbon in both electrolytes (*i.e.* KOH and H_2SO_4). The practical applicability of the Fe-N-doped catalyst has been shown by assembling an AAEMFC with a performance matching that of another AAEMFC based on a Pt/C cathode catalyst.

Experimental Section

Preparation of mesoporous Fe-N-doped carbon capsules

The N-doped carbon capsules were fabricated as reported first by our group.[46] Briefly, silica particles with a hollow core and a mesoporous shell (SCMS) were synthesized as reported by Unger *et al.*[74] Afterwards, the SCMS particles were impregnated by the drop-wise impregnation technique with a 2 M $FeCl_3$ ethanol solution (around 0.27 g $FeCl_3$ / g silica). Then, the impregnated sample was exposed to pyrrole (Aldrich, 99%) vapors at 25 ºC for 22 h in a closed vessel. The dark solid thus obtained was heated under N_2 to 850 ºC (3 ºC min^{-1}) for 1 h.

Finally, the carbonized composite was treated with hydrofluoric acid for four days to dissolve the silica framework. The carbon residue was collected by filtration, washed with distilled water, and dried at 120 ºC for several hours. The carbon capsules with nitrogen functionalities have been designated as *Fe-N-CC*.

Characterization of materials

The morphology of the powders was examined by scanning (SEM, Zeiss DSM 942) and transmission (HRTEM, JEOL (JEM 2100-F)) electron microscopy. Nitrogen sorption isotherms were performed at -196 ºC in a Micromeritics ASAP 2020 volumetric adsorption system. The Brunauer-Emmett-Teller (BET) surface area was deduced from an analysis of the isotherm in the relative pressure range of 0.04-0.20. The total pore volume was calculated from the amount of nitrogen adsorbed at a relative pressure of 0.90. The mesopore size distribution was calculated by means of the Kruk-Jaroniec-Sayari (KJS) method.[75] The primary mesopore volume (V_m) and external surface area (S_{ext}) were estimated using the α_s-plot method. The reference adsorption data used for the α_s analysis of the carbon sample correspond to a non-graphitized carbon black sample.[76]

The thermogravimetric analysis was performed on a CI Electronics system. Raman spectra were recorded on a Horiva (LabRamHR-800) spectrometer. The source of radiation was a laser operating at a wavelength of 514 nm and at a power of 25 mW. Calculation of the parameters I_D/I_G (integrated intensity ratio) and width at half maximum (FWHM) of the G band was done by the deconvolution of the spectra. The curve fitting was performed with the combination of Gaussian-Lorentzian line shaped that gave the minimum fitting

error. X-ray photoelectron spectroscopy (XPS) was performed on a Specs spectrometer, using Mg Kα (1253.6 eV) radiation from a double anode at 150 W. Binding energies for the high resolution spectra were calibrated by setting C 1s to 284.4 eV. X-ray diffraction (XRD) patterns were obtained on a Siemens D5000 instrument operating at 40 kV and 20 mA and using Cu Kα radiation (λ=0.15406 nm). Bulk elemental analysis (C, H, N and O) of the samples was carried out on a LECO CHN-932 microanalyzer. The bulk Fe content in the catalysts was obtained by ICP-MS analysis in a 7700x equipment (Agilent).

The electrical conductivity of the carbon materials was determined by pressing the powdered material at 7.1 MPa.

Electrochemical measurements

Electrochemical measurements were conducted using an AUTOLAB PGSTAT 101 and a Multi AUTOLAB M101 (CH Instruments). Fe-N-CC catalyst inks were prepared by ultrasonically dispersing 1.5 mg of Fe-N-CC catalyst in a solution containing 100 µL Nafion (5 wt %) solution and 900 µL deionized water. For comparison, the Pt/C catalyst (20 wt % Pt on graphitized carbon, Sigma-Aldrich) ink was prepared in the same way, using the same amount of catalyst (*i.e*. 1.5 mg). The mass loading of both catalysts is the same, *i.e.* 0.1 mg cm^{-2}. The above prepared catalyst inks were deposited onto a polished glassy carbon electrode (α-Al_2O_3 slurry, 50 nm) and dried under room temperature. A conventional three-electrode cell was employed, incorporating Ag/AgCl (3 M KCl) as the reference electrode, a Pt wire as the counter electrode and a rotating disk electrode (RDE) or rotating ring-disk electrode (RRDE) coated with the catalyst film as the working electrode. The electrolyte was 0.5 M H_2SO_4

solution or 0.1 M KOH solution. All the experiments were carried out at 20 ºC. Before testing, O_2/N_2 gas was bubbled through the electrolyte in the cell for 30 min to saturate it with O_2/N_2. The measured potentials *vs.* Ag/AgCl (3 M KCl) were converted to the reversible hydrogen electrode (RHE) scale according to the Nernst equation:

$$E_{RHE} = E_{Ag/AgCl} + 0.059\ pH + E^{o}_{Ag/AgCl} \quad (1)$$

where $E_{Ag/AgCl}$ is the experimentally measured potential *vs.* Ag/AgCl reference and $E^{o}_{Ag/AgCl}$ = 0.21 V at 20 ºC. The values of potential provided along the text are referenced against RHE unless otherwise stated.

Cyclic voltammetry (CV) was performed from 0 to 1.2 V *vs.* RHE in O_2- and N_2-saturated 0.1 M KOH and 0.5 M H_2SO_4 electrolytes, with a sweep rate of 100 mV s^{-1}.

RDE linear sweep voltammetry (LSV) measurements were conducted from 1.2 to 0 V *vs.* RHE in O_2-saturated 0.1 M KOH and 0.5 M H_2SO_4 electrolytes at a scan rate of 10 mV s^{-1} under disk rotation rates of 400, 800, 1200, 1600, 2000 and 2400 rpm. The working electrode was a 3.0 mm diameter GC rotating disk electrode.

The apparent number of electrons transferred during ORR on the carbon catalysts was determined by the Koutechy-Levich equation given by:

$$\frac{1}{J}=\frac{1}{J_L}+\frac{1}{J_K}=\frac{1}{B\omega^{1/2}}+\frac{1}{J_K} \quad (2)$$

$$B=0.62nFC_0(D_0)^{2/3}\nu^{\frac{1}{6}} \quad (3)$$

where J is the measured current density, J_K is the kinetic current density, J_L is the diffusion-limited current density, ω is the electrode rotation rate, *F* is the Faraday constant (96485 C mol^{-1}), C_0 is the bulk concentration of O_2 (1.1×10^{-3}

mol L^{-1} for 0.5 M H_2SO_4 solution and 1.2 x10^{-3} mol L^{-1} 0.1 M KOH solution), D_0 is the diffusion coefficient of O_2 (1.4 x 10^{-5} cm^2 s^{-1} for 0.5 M H_2SO_4 solution and 1.9 x 10^{-5} cm^2 s^{-1} for 0.1 M KOH solution) and ν is the kinetic viscosity of the electrolyte (0.01 cm^2 s^{-1} for both 0.5 M H_2SO_4 solution and 0.1 M KOH solution).[77-79]

For the RRDE tests, the disk potential was scanned at 10 mV s^{-1}, while the ring potential was held at 1.5 V *vs.* RHE in order to oxidize any H_2O_2 produced.[8, 80] The working electrode was a 5 mm GC disk electrode and a Pt ring electrode (375 μm gap). The H_2O_2 collection efficiency at the ring (*N*=0.249) was provided by the manufacturer. The following equations were used to calculate *n* (the apparent number of electrons transferred during ORR) and % H_2O_2 (the percentage of H_2O_2 released during ORR): [81]

$$n = \frac{4\, I_D}{I_D + \left(\frac{I_R}{N}\right)} \tag{4}$$

$$\%\, H_2O_2 = 100\frac{2\frac{I_R}{N}}{I_D + \left(\frac{I_R}{N}\right)} \tag{5}$$

where I_D is the Faradaic current at the disk, I_R is the Faradaic current at the ring, *N* is the H_2O_2 collection coefficient at the ring.

The stability of the catalyst was assessed by means of an US Department of Energy's accelerated durability test protocol by cycling the catalysts between 0.6 and 1.0 V (*vs.* RHE) at 50 mV s^{-1} under N_2 atmosphere in 0.1 M KOH and 0.5 M H_2SO_4.[27, 31]

Fuel cell assembly. The electrodes were prepared by spray-coating the catalyst ink on A201 alkaline membrane (Tokoyama, anion exchange capacity: 1.7 mmol g^{-1}, thickness: 28 μm) at 40°C. The catalyst ink was prepared by

ultrasonicating the desired amount of catalyst in 2-propanol solution (Sigma-Aldrich) and AS-4 ionomer (Tokuyama, 5 wt % solution, anion exchange capacity: 1.5 mmol g^{-1}) for 30 minutes. The amount of AS-4 ionomer was kept at 20 wt % for Fe-N-CC catalyst and 15 wt % for commercial Pt/C (Sigma Aldrich, 20 wt % Pt on graphitized carbon). The catalyst loading was calculated by weighing the membrane before and after spray-coating, and kept at 0.2 mg cm^{-2} (total catalyst). Commercial Pt/C (Alfa Aesar, Pt 40 wt %) catalyst was used as the anode catalyst with the loading fixed at 0.4 mg_{Pt} cm^{-2}. The effective electrode area was 5.29 cm^2. The catalyst coated membrane (CCM) was soaked in 0.1 M KOH overnight before testing.

Each CCM was tested by fitting it between two gas diffusion layers and mounted in single-cell hardware with a built-in reference electrode (Fuel Cell Technologies Inc.). Fuel cell measurements were carried out using Scribner 890e test station (Scribner Associates). Electrochemical impedance spectroscopy (EIS) measurements were carried out using Gamry Reference 3000AE (Gamry Instruments) in a three-electrode configuration to monitor both the anode and cathode individually. The cell temperature was set at 50°C, and the anode and cathode were fed with humidified (95% relative humidity) H_2 and O_2 at 0.5 L min^{-1} and 1 L min^{-1}, respectively. Prior to measurements, the CCM was activated by maintaining the cell voltage at ~0.3 V for 1 hour. The EIS was done at 10, 25, 50, and 100 mA cm^{-2} in a frequency range of 0.1 – 10 kHz with applied AC amplitude of 10% of the actual current.

Acknowledgments

This research work was supported by the Spanish Ministerio de Economía y Competitividad, MINECO (MAT2012-31651), Fondo Europeo de Desarrollo Regional (FEDER) and FICYT Regional Project (GRUPIN14-102). G. A. F. thanks the MINECO for his predoctoral contract and M. S. thanks the Spanish Ministerio de Ciencia e Innovación for her Ramón y Cajal contract.

Supporting Information Available: Comparative tables of N-doped and Fe-N-doped carbon materials in basic and acid media. Nitrogen sorption isotherm, XRD pattern, Raman spectra of and graphitic carbon regions, TGA analysis in air. XPS general spectrum and high-resolution Fe $2p_{3/2}$ XPS spectrum. TEM image and its corresponding EDX mappings for C, N, O and Fe. HRTEM images of Fe_3C nanoparticle. Cyclic voltammograms in N_2 and O_2 saturated 0.1 M KOH and 0.5 M H_2SO_4 electrolytes, LSV at 10 mV s^{-1} in the presence of oxygen with rotation speed from 400 to 2400 rpm in 0.1 M KOH and 0.5 M H_2SO_4, Koutecky-Levich plots in 0.1 M KOH and 0.1 M H_2SO_4, comparison of the chronoamperometric response of Fe-N-CC and Pt/C over 10,000 s at 0.68 V and a constant rotation speed of 800 rpm in O_2-saturated solution 0.1 M KOH, and Nyquist plots of the whole cell, including the half-cell measurements of the cathode This material is available free of charge *via* the Internet at http://pubs.acs.org.

List of Tables and Figures

Table 1. Physico-chemical properties of the N-doped carbon capsules.

Sample code	S_{BET} ($m^2\ g^{-1}$)	V_p ($cm^3\ g^{-1}$)[a]	Pore size (nm)[b]	α_s-plot results		C (wt %)	N (wt %)	O (wt %)	σ ($S\ m^{-1}$)
				V_m ($cm^3\ g^{-1}$)[c]	S_{ext} ($m^2\ g^{-1}$)[d]				
Fe-N-CC	1590	1.46	3.8	1.28	92	83.28	5.88	10.04	22

[a] Pore volume determined at p/p_0=0.90. [b] Maximum of the KJS pore size distribution. [c] Volume of framework-confined mesopores. [d] External surface area.

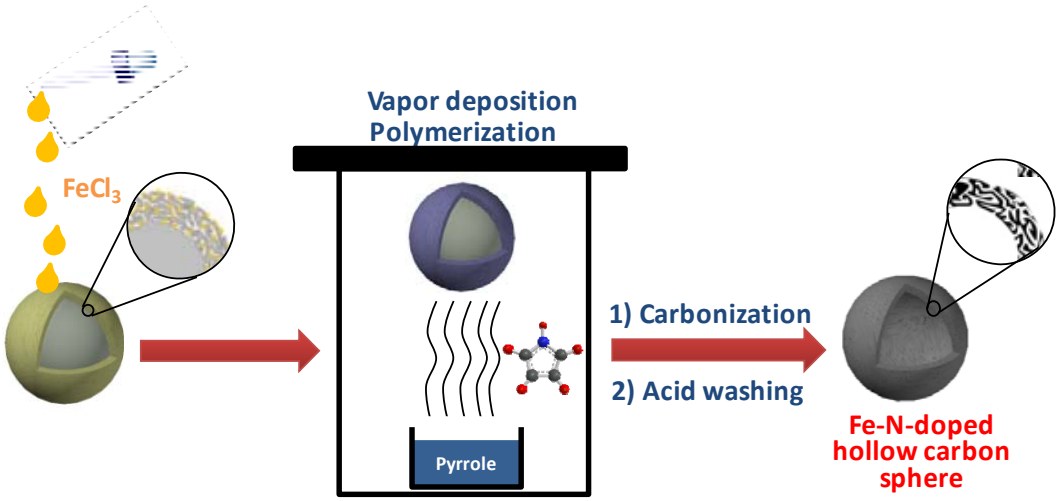

Figure 1. Schematic illustration of the synthesis procedure.

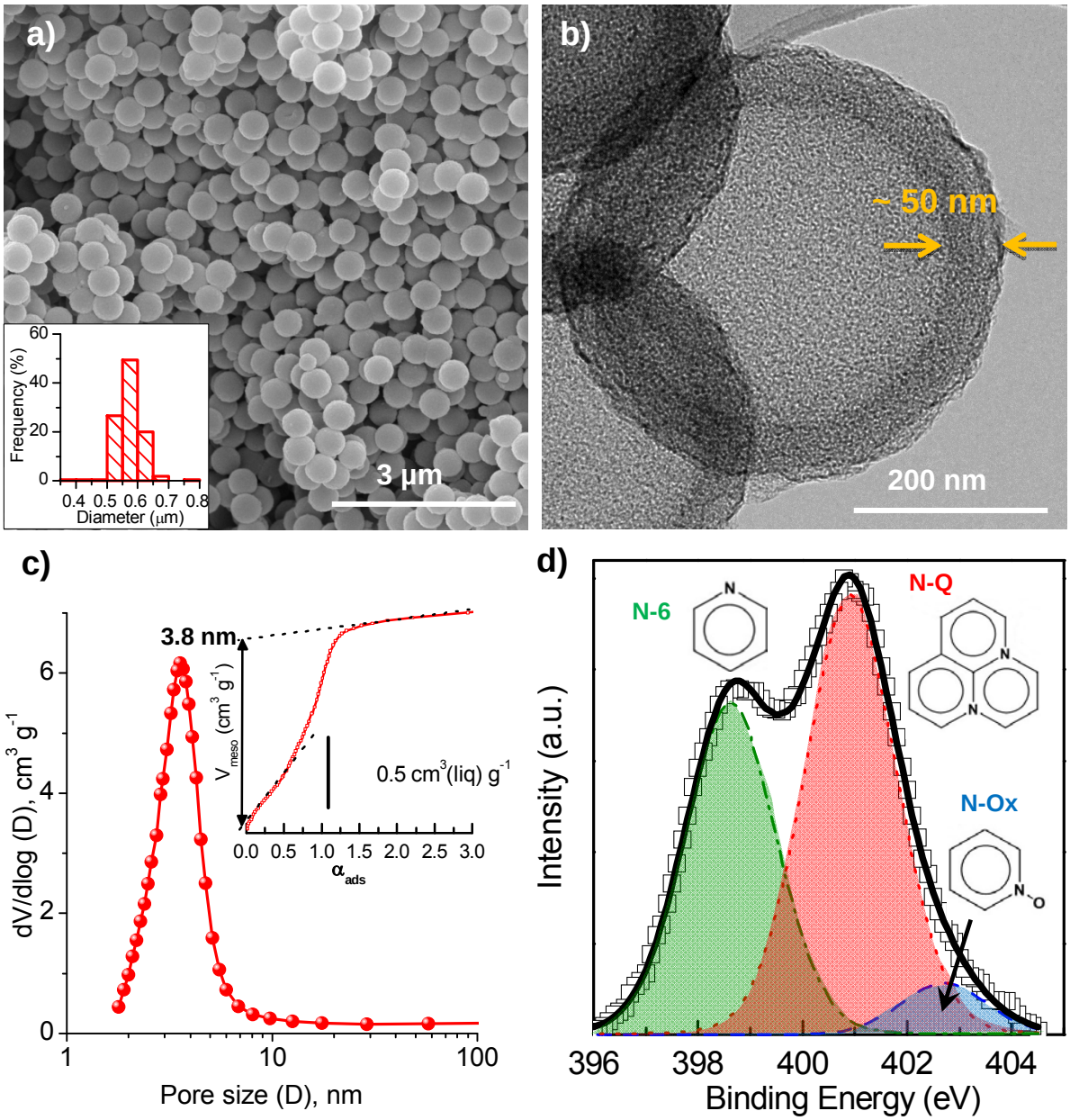

Figure 2. (a) SEM image of the hollow carbon capsules (inset: particle diameter distribution determined over 200 particles), (b) high-magnification TEM images of the hollow carbon capsules, (c) KJS pore size distribution and α_s-plot method applied to the N_2 adsorption branch (inset) and (d) XPS N 1s core level spectra of the Fe-N-doped carbon capsules (Fe-N-CC).

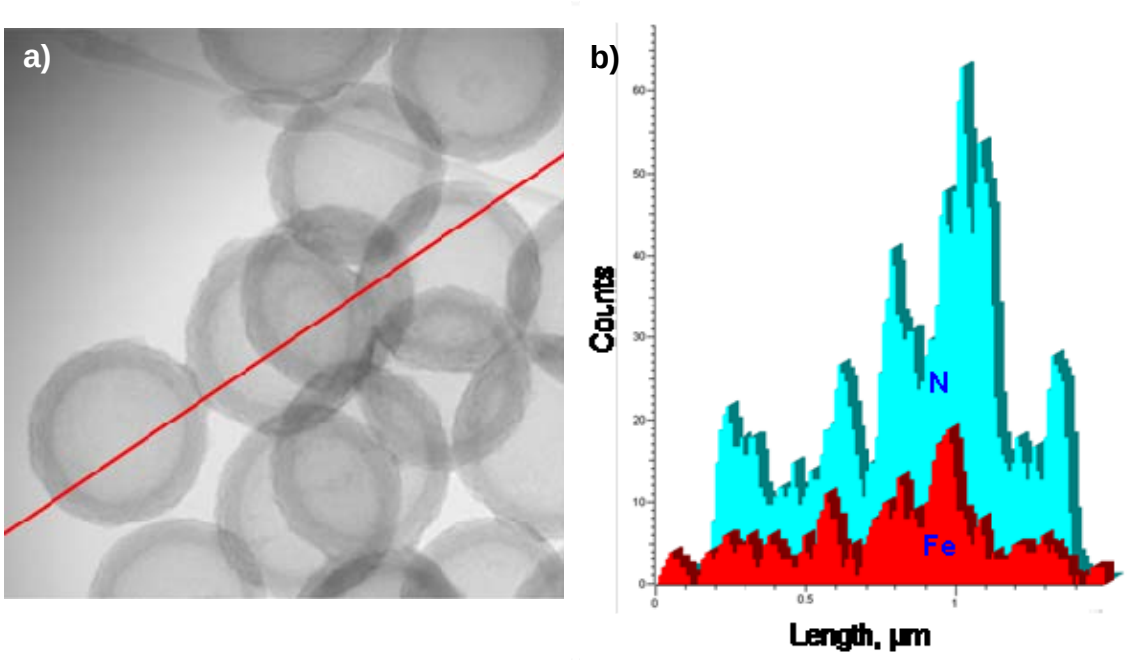

Figure 3. (a) TEM image of the Fe-N-CC carbon material and (b) its corresponding line profile concentration for nitrogen and iron.

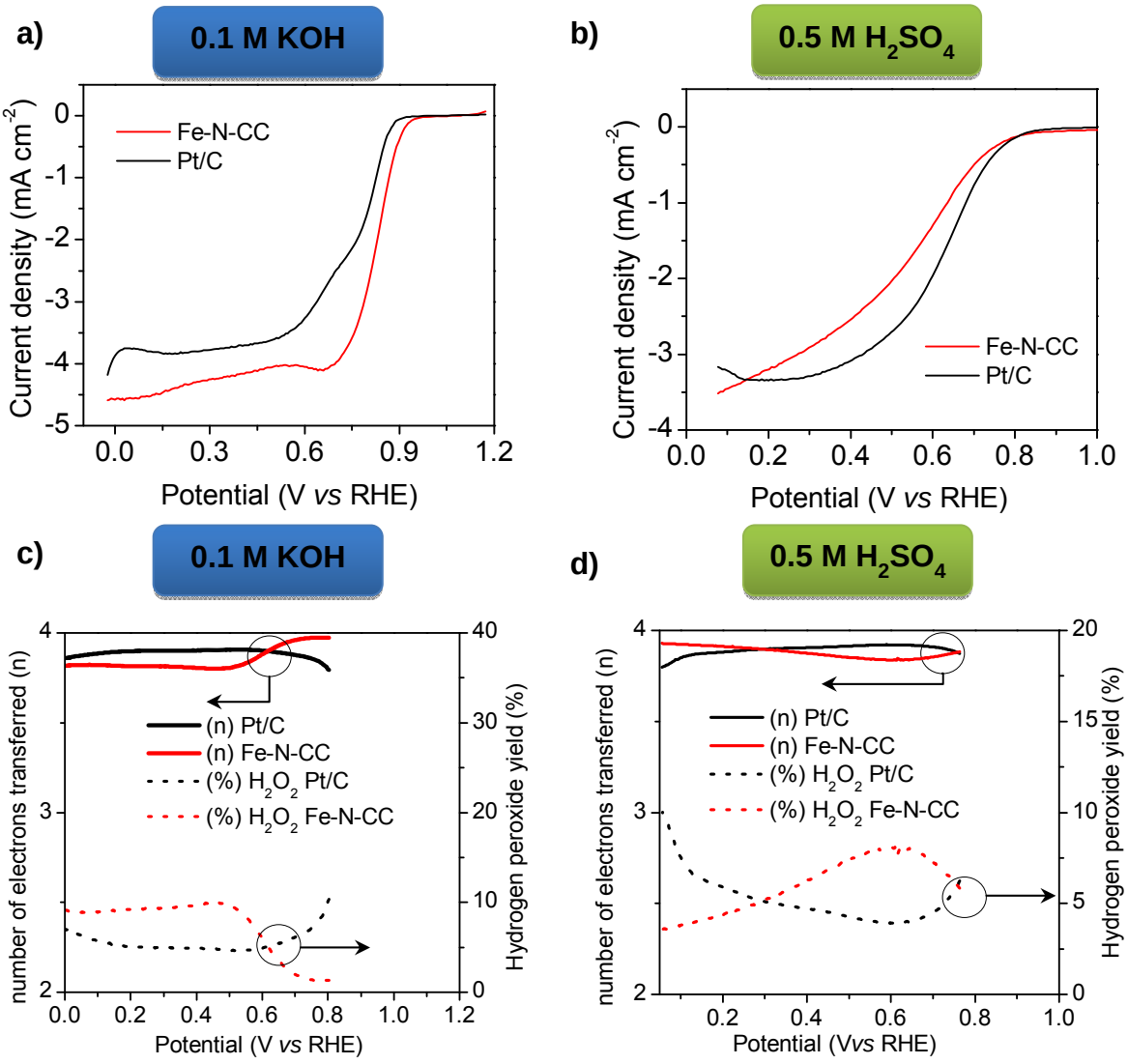

Figure 4. Comparison of the RDE polarization curves at 1600 rpm for Fe-N-CC and Pt/C catalysts in (a) 0.1 M KOH and (b) 0.1 M H_2SO_4, and number of electrons transferred and peroxide yield of the Fe-N-CC carbon capsules and Pt/C catalysis in (c) 0.1 M KOH and (d) 0.5 M H_2SO_4. The catalyst loadings were 0.1 mg cm^{-2} for both Fe-N-CC and Pt/C catalysts.

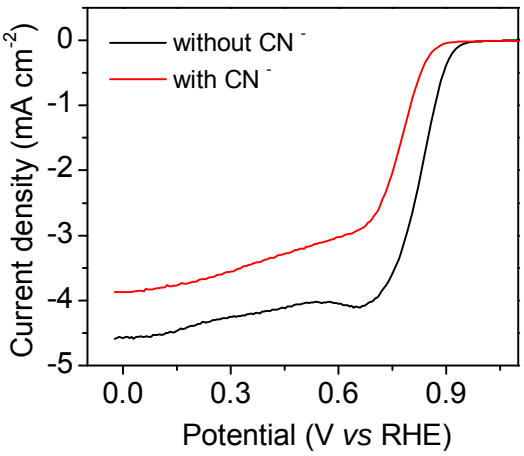

Figure 5. LSVs at 10 mV s^{-1} in the presence of oxygen at 1600 rpm in 0.1 M KOH without and in presence of cyanide ions (10 mM KCN).

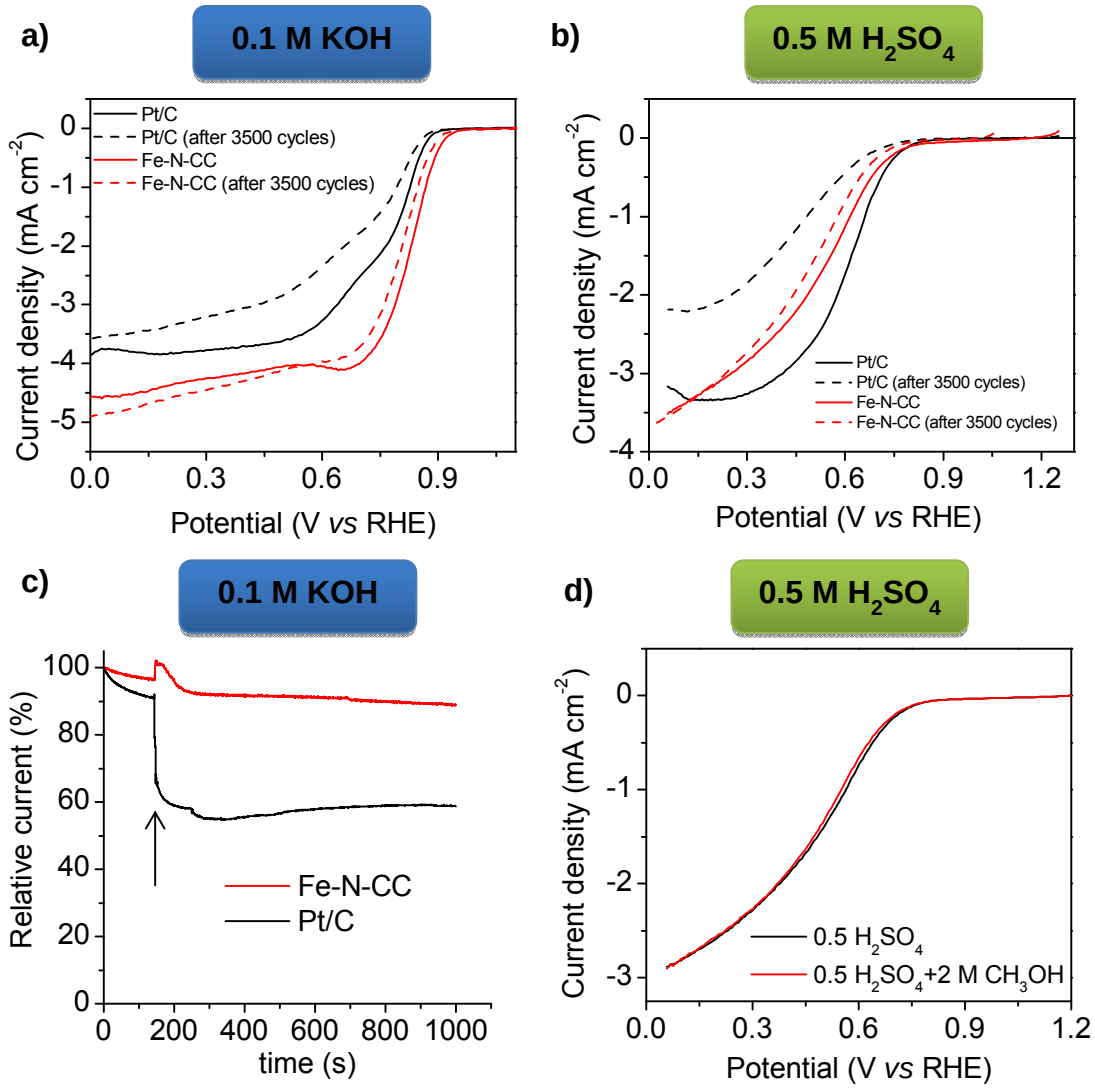

Figure 6. LSVs for Fe-N-CC and Pt/C at 1600 rpm in O_2-saturated (a) 0.1 M KOH and (b) 0.5 M H_2SO_4 before and after 3500 potential cycles, (c) comparison of the chronoamperometric response over 1000 s at a constant rotation speed of 1600 rpm in O_2-saturated solution at 0.68 V for Fe-N-CC and Pt/C catalysts in 0.1 M KOH (the arrow indicates the addition of methanol) and (d) polarization curves of Fe-N-CC in O_2-saturated 0.5 M H_2SO_4 with (black) and without (red) 2 M methanol.

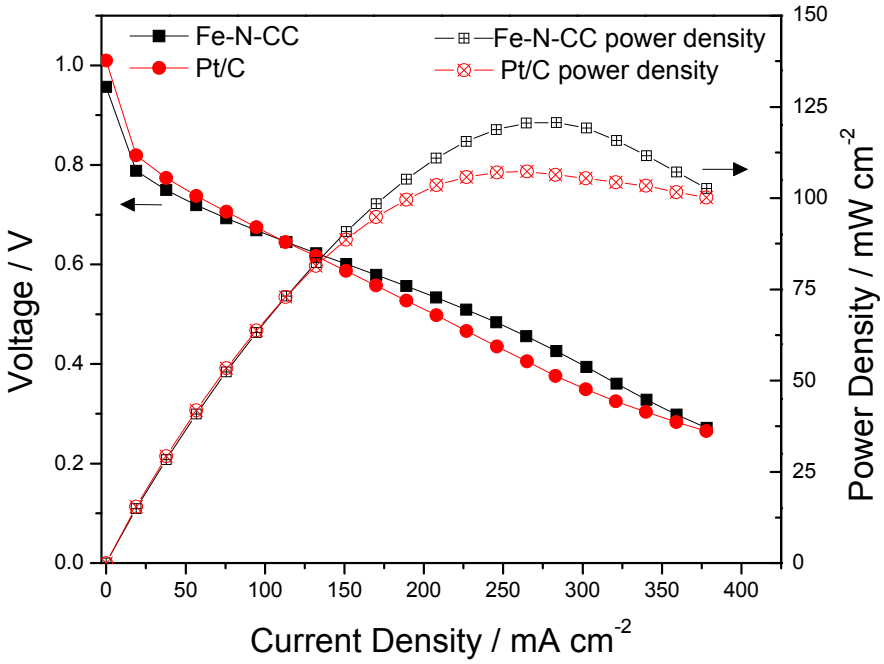

Figure 7. Polarization curve and power density of alkaline exchange membrane fuel cells operating at 50°C with Fe-N-CC and Pt/C as cathode catalysts (0.2 mg cm^{-2}).

References

1. Marković, N. M.; Schmidt, T. J.; Stamenković, V.; Ross, P. N. Oxygen Reduction Reaction on Pt and Pt Bimetallic Surfaces: A Selective Review. *Fuel Cells* **2001**, 1, 105-116.
2. Chen, Z.; Higgins, D.; Yu, A.; Zhang, L.; Zhang, J. A review on non-precious metal electrocatalysts for PEM fuel cells. *Energy Environ. Sci.* **2011**, 4, 3167-3192.
3. Yu, D.; Nagelli, E.; Du, F.; Dai, L. Metal-Free Carbon Nanomaterials Become More Active than Metal Catalysts and Last Longer. *J. Phys. Chem. Lett.* **2010**, 1, 2165-2173.
4. Zhu, J.; Yang, D.; Yin, Z.; Yan, Q.; Zhang, H. Graphene and Graphene-Based Materials for Energy Storage Applications. *Small* **2014**, 10, 3480-3498.
5. Othman, R.; Dicks, A. L.; Zhu, Z. Non precious metal catalysts for the PEM fuel cell cathode. *Int. J. Hydrogen Energy* **2012**, 37, 357-372.
6. Jaouen, F.; Proietti, E.; Lefevre, M.; Chenitz, R.; Dodelet, J.-P.; Wu, G.; Chung, H. T.; Johnston, C. M.; Zelenay, P. Recent advances in non-precious metal catalysis for oxygen-reduction reaction in polymer electrolyte fuel cells. *Energy Environ. Sci.* **2011**, 4, 114-130.
7. Gorlin, Y.; Chung, C.-J.; Nordlund, D.; Clemens, B. M.; Jaramillo, T. F. Mn3O4 Supported on Glassy Carbon: An Active Non-Precious Metal Catalyst for the Oxygen Reduction Reaction. *ACS Catalysis* **2012**, 2, 2687-2694.
8. Hu, Y.; Jensen, J. O.; Zhang, W.; Cleemann, L. N.; Xing, W.; Bjerrum, N. J.; Li, Q. Hollow spheres of iron carbide nanoparticles encased in graphitic layers as oxygen reduction catalysts. *Angew. Chem. Int. Ed.* **2014**, 53, 3675-3679.
9. Dai, L.; Xue, Y.; Qu, L.; Choi, H.-J.; Baek, J.-B. Metal-Free Catalysts for Oxygen Reduction Reaction. *Chem. Rev.* **2015**, 115, 4823-4892.
10. Gong, K.; Du, F.; Xia, Z.; Durstock, M.; Dai, L. Nitrogen-Doped Carbon Nanotube Arrays with High Electrocatalytic Activity for Oxygen Reduction. *Science* **2009**, 323, 760-764.
11. Masa, J.; Xia, W.; Muhler, M.; Schuhmann, W. On the Role of Metals in Nitrogen-Doped Carbon Electrocatalysts for Oxygen Reduction. *Angew. Chem. Int. Ed.* **2015**, 54, 10102-10120.
12. Wang, D.-W.; Su, D. Heterogeneous nanocarbon materials for oxygen reduction reaction. *Energy Environ. Sci.* **2014**, 7, 576-591.
13. Daems, N.; Sheng, X.; Vankelecom, I. F. J.; Pescarmona, P. P. Metal-free doped carbon materials as electrocatalysts for the oxygen reduction reaction. *J. Mater. Chem. A* **2014**, 2, 4085-4110.
14. Shao, Y.; Sui, J.; Yin, G.; Gao, Y. Nitrogen-doped carbon nanostructures and their composites as catalytic materials for proton exchange membrane fuel cell. *Appl. Catal. B* **2008**, 79, 89-99.
15. Qu, L.; Liu, Y.; Baek, J.-B.; Dai, L. Nitrogen-Doped Graphene as Efficient Metal-Free Electrocatalyst for Oxygen Reduction in Fuel Cells. *ACS Nano* **2010**, 4, 1321-1326.
16. Wu, K.-H.; Wang, D.-W.; Su, D.-S.; Gentle, I. R. A Discussion on the Activity Origin in Metal-Free Nitrogen-Doped Carbons For Oxygen Reduction Reaction and their Mechanisms. *ChemSusChem* **2015**, 8, 2772-2788.

17. Yu, X.; Ye, S. Recent advances in activity and durability enhancement of Pt/C catalytic cathode in PEMFC: Part II: Degradation mechanism and durability enhancement of carbon supported platinum catalyst. *J. Power Sources* **2007**, 172, 145-154.
18. Yin, J.; Qiu, Y.; Yu, J. Enhanced electrochemical activity for oxygen reduction reaction from nitrogen-doped carbon nanofibers by iron doping. *ECS Solid State Let.* **2013**, 2, M37-M39.
19. Mo, Z.; Liao, S.; Zheng, Y.; Fu, Z. Preparation of nitrogen-doped carbon nanotube arrays and their catalysis towards cathodic oxygen reduction in acidic and alkaline media. *Carbon* **2012**, 50, 2620-2627.
20. Vikkisk, M.; Kruusenberg, I.; Joost, U.; Shulga, E.; Tammeveski, K. Electrocatalysis of oxygen reduction on nitrogen-containing multi-walled carbon nanotube modified glassy carbon electrodes. *Electrochim. Acta* **2013**, 87, 709-716.
21. Chen, Y.; Ma, R.; Zhou, Z.; Liu, G.; Zhou, Y.; Liu, Q.; Kaskel, S.; Wang, J. An In Situ Source-Template-Interface Reaction Route to 3D Nitrogen-Doped Hierarchical Porous Carbon as Oxygen Reduction Electrocatalyst. *Advanced Materials Interfaces* **2015**, 2.
22. Liang, J.; Zheng, Y.; Chen, J.; Liu, J.; Hulicova-Jurcakova, D.; Jaroniec, M.; Qiao, S. Z. Facile Oxygen Reduction on a Three-Dimensionally Ordered Macroporous Graphitic C3N4/Carbon Composite Electrocatalyst. *Angew. Chem. Int. Ed.* **2012**, 51, 3892-3896.
23. Cong, H.-P.; Wang, P.; Gong, M.; Yu, S.-H. Facile synthesis of mesoporous nitrogen-doped graphene: An efficient methanol–tolerant cathodic catalyst for oxygen reduction reaction. *Nano Energy* **2014**, 3, 55-63.
24. Chen, P.; Wang, L.-K.; Wang, G.; Gao, M.-R.; Ge, J.; Yuan, W.-J.; Shen, Y.-H.; Xie, A.-J.; Yu, S.-H. Nitrogen-doped nanoporous carbon nanosheets derived from plant biomass: an efficient catalyst for oxygen reduction reaction. *Energy Environ. Sci.* **2014**, 7, 4095-4103.
25. Zhou, M.; Yang, C.; Chan, K.-Y. Structuring Porous Iron-Nitrogen-Doped Carbon in a Core/Shell Geometry for the Oxygen Reduction Reaction. *Adv. Energy Mater.* **2014**, 4.
26. Zhong, H.; Deng, C.; Qiu, Y.; Yao, L.; Zhang, H. Nitrogen-doped hierarchically porous carbon as efficient oxygen reduction electrocatalysts in acid electrolyte. *J. Mater. Chem. A* **2014**, 2, 17047-17057.
27. Li, Y.; Zhou, W.; Wang, H.; Xie, L.; Liang, Y.; Wei, F.; Idrobo, J.-C.; Pennycook, S. J.; Dai, H. An oxygen reduction electrocatalyst based on carbon nanotube-graphene complexes. *Nat Nano* **2012**, 7, 394-400.
28. Zhang, J.; Zhao, Z.; Xia, Z.; Dai, L. A metal-free bifunctional electrocatalyst for oxygen reduction and oxygen evolution reactions. *Nat Nano* **2015**, 10, 444-452.
29. Yu, D.; Zhang, Q.; Dai, L. Highly Efficient Metal-Free Growth of Nitrogen-Doped Single-Walled Carbon Nanotubes on Plasma-Etched Substrates for Oxygen Reduction. *J. Am. Chem. Soc.* **2010**, 132, 15127-15129.
30. Parvez, K.; Yang, S.; Hernandez, Y.; Winter, A.; Turchanin, A.; Feng, X.; Müllen, K. Nitrogen-Doped Graphene and Its Iron-Based Composite As Efficient Electrocatalysts for Oxygen Reduction Reaction. *ACS Nano* **2012**, 6, 9541-9550.

31. Wu, G.; More, K. L.; Johnston, C. M.; Zelenay, P. High-Performance Electrocatalysts for Oxygen Reduction Derived from Polyaniline, Iron, and Cobalt. *Science* **2011**, 332, 443-447.
32. Masa, J.; Zhao, A.; Xia, W.; Sun, Z.; Mei, B.; Muhler, M.; Schuhmann, W. Trace metal residues promote the activity of supposedly metal-free nitrogen-modified carbon catalysts for the oxygen reduction reaction. *Electrochem. Commun.* **2013**, 34, 113-116.
33. Jin, X.; Zhang, G.; Hao, Y.; Chang, Z.; Sun, X. Residual metals present in "metal-free" N-doped carbons. *Chem. Commun.* **2015**, 51, 15585-15587.
34. Ranjbar Sahraie, N.; Paraknowitsch, J. P.; Göbel, C.; Thomas, A.; Strasser, P. Noble-Metal-Free Electrocatalysts with Enhanced ORR Performance by Task-Specific Functionalization of Carbon using Ionic Liquid Precursor Systems. *J. Am. Chem. Soc.* **2014**, 136, 14486-14497.
35. Lin, L.; Zhu, Q.; Xu, A.-W. Noble-Metal-Free Fe–N/C Catalyst for Highly Efficient Oxygen Reduction Reaction under Both Alkaline and Acidic Conditions. *J. Am. Chem. Soc.* **2014**, 136, 11027-11033.
36. Sevilla, M.; Yu, L.; Fellinger, T. P.; Fuertes, A. B.; Titirici, M.-M. Polypyrrole-derived mesoporous nitrogen-doped carbons with intrinsic catalytic activity in the oxygen reduction reaction. *RSC Adv.* **2013**, 3, 9904-9910.
37. Chao, S.; Lu, Z.; Bai, Z.; Cui, Q.; Qiao, J.; Yang, Z.; Yang, L. Tuning synthesis of highly active nitrogen-doped graphite and determining the optimal structure from first-principles calculations. *Int. J. Electrochem. Sci* **2013**, 8, 8786-8799.
38. Wu, Z.-Y.; Xu, X.-X.; Hu, B.-C.; Liang, H.-W.; Lin, Y.; Chen, L.-F.; Yu, S.-H. Iron Carbide Nanoparticles Encapsulated in Mesoporous Fe-N-Doped Carbon Nanofibers for Efficient Electrocatalysis. *Angew. Chem. Int. Ed.* **2015**, 54, 8179-8183.
39. Sevilla, M.; Fuertes, A. B. Catalytic graphitization of templated mesoporous carbons. *Carbon* **2006**, 44, 468-474.
40. Sevilla, M.; Sanchis, C.; Valdes-Solis, T.; Morallon, E.; Fuertes, A. B. Synthesis of graphitic carbon nanostructures from sawdust and their application as electrocatalyst supports. *J. Phys. Chem. C.* **2007**, 111, 9749-9756.
41. Ōya, A.; Marsh, H. Phenomena of catalytic graphitization. *J. Mater. Sci.* **1982**, 17, 309-322.
42. Pels, J. R.; Kapteijn, F.; Moulijn, J. A.; Zhu, Q.; Thomas, K. M. Evolution of nitrogen functionalities in carbonaceous materials during pyrolysis. *Carbon* **1995**, 33, 1641-1653.
43. Schmiers, H.; Friebel, J.; Streubel, P.; Hesse, R.; Köpsel, R. Change of chemical bonding of nitrogen of polymeric N-heterocyclic compounds during pyrolysis. *Carbon* **1999**, 37, 1965-1978.
44. Tylus, U.; Jia, Q.; Strickland, K.; Ramaswamy, N.; Serov, A.; Atanassov, P.; Mukerjee, S. Elucidating Oxygen Reduction Active Sites in Pyrolyzed Metal–Nitrogen Coordinated Non-Precious-Metal Electrocatalyst Systems. *J. Phys. Chem. C.* **2014**, 118, 8999-9008.
45. Wei, J.; Liang, Y.; Hu, Y.; Kong, B.; Simon, G. P.; Zhang, J.; Jiang, S. P.; Wang, H. A Versatile Iron–Tannin-Framework Ink Coating Strategy to Fabricate Biomass-Derived Iron Carbide/Fe-N-Carbon Catalysts for Efficient Oxygen Reduction. *Angew. Chem. Int. Ed.* **2016**, 55, 1355-1359.

46. Ferrero, G. A.; Fuertes, A. B.; Sevilla, M. N-doped porous carbon capsules with tunable porosity for high-performance supercapacitors. *J. Mater. Chem. A* **2015**, 3, 2914-2923.
47. Liu, R.; Wu, D.; Feng, X.; Müllen, K. Nitrogen-Doped Ordered Mesoporous Graphitic Arrays with High Electrocatalytic Activity for Oxygen Reduction. *Angew. Chem. Int. Ed.* **2010**, 49, 2565-2569.
48. He, W.; Jiang, C.; Wang, J.; Lu, L. High-Rate Oxygen Electroreduction over Graphitic-N Species Exposed on 3D Hierarchically Porous Nitrogen-Doped Carbons. *Angew. Chem. Int. Ed.* **2014**, 53, 9503-9507.
49. Wei, W.; Liang, H.; Parvez, K.; Zhuang, X.; Feng, X.; Müllen, K. Nitrogen-Doped Carbon Nanosheets with Size-Defined Mesopores as Highly Efficient Metal-Free Catalyst for the Oxygen Reduction Reaction. *Angew. Chem.* **2014**, 126, 1596-1600.
50. You, C.; Liao, S.; Qiao, X.; Zeng, X.; Liu, F.; Zheng, R.; Song, H.; Zeng, J.; Li, Y. Conversion of polystyrene foam to a high-performance doped carbon catalyst with ultrahigh surface area and hierarchical porous structures for oxygen reduction. *J. Mater. Chem. A* **2014**, 2, 12240-12246.
51. Liu, J.; Sun, X.; Song, P.; Zhang, Y.; Xing, W.; Xu, W. High-Performance Oxygen Reduction Electrocatalysts based on Cheap Carbon Black, Nitrogen, and Trace Iron. *Adv. Mater.* **2013**, 25, 6879-6883.
52. Zhang, C.; Antonietti, M.; Fellinger, T.-P. Blood Ties: Co3O4 Decorated Blood Derived Carbon as a Superior Bifunctional Electrocatalyst. *Adv. Funct. Mater.* **2014**, 24, 7655-7665.
53. Wu, Z.; Li, W.; Xia, Y.; Webley, P.; Zhao, D. Ordered mesoporous graphitized pyrolytic carbon materials: synthesis, graphitization, and electrochemical properties. *J. Mater. Chem.* **2012**, 22, 8835-8845.
54. Tang, J.; Liu, J.; Li, C.; Li, Y.; Tade, M. O.; Dai, S.; Yamauchi, Y. Synthesis of Nitrogen-Doped Mesoporous Carbon Spheres with Extra-Large Pores through Assembly of Diblock Copolymer Micelles. *Angew. Chem. Int. Ed.* **2015**, 54, 588-593.
55. Xiao, H.; Shao, Z.-G.; Zhang, G.; Gao, Y.; Lu, W.; Yi, B. Fe–N–carbon black for the oxygen reduction reaction in sulfuric acid. *Carbon* **2013**, 57, 443-451.
56. Liu, X.; Zhu, H.; Yang, X. One-step synthesis of dopamine-derived micro/mesoporous nitrogen-doped carbon materials for highly efficient oxygen-reduction catalysts. *J. Power Sources* **2014**, 262, 414-420.
57. Yang, T.; Liu, J.; Zhou, R.; Chen, Z.; Xu, H.; Qiao, S. Z.; Monteiro, M. J. N-doped mesoporous carbon spheres as the oxygen reduction reaction catalysts. *J. Mater. Chem. A* **2014**, 2, 18139-18146.
58. Li, J.; Li, Z.; Tong, J.; Xia, C.; Li, F. Nitrogen-doped ordered mesoporous carbon sphere with short channel as an efficient metal-free catalyst for oxygen reduction reaction. *RSC Adv.* **2015**, 5, 70010-70016.
59. Hu, C.; Wang, L.; Zhao, Y.; Ye, M.; Chen, Q.; Feng, Z.; Qu, L. Designing nitrogen-enriched echinus-like carbon capsules for highly efficient oxygen reduction reaction and lithium ion storage. *Nanoscale* **2014**, 6, 8002-8009.
60. Shih, Y.-H.; Sagar, G. V.; Lin, S. D. Effect of Electrode Pt Loading on the Oxygen Reduction Reaction Evaluated by Rotating Disk Electrode and Its Implication on the Reaction Kinetics. *J. Phys. Chem. C.* **2008**, 112, 123-130.
61. Alonso-Vante, N. Platinum and Non-Platinum Nanomaterials for the Molecular Oxygen Reduction Reaction. *ChemPhysChem* **2010**, 11, 2732-2744.

62. Zhang, J. *PEM fuel cell electrocatalysts and catalyst layers: fundamentals and applications*. Springer Science & Business Media: 2008.
63. Thorum, M. S.; Hankett, J. M.; Gewirth, A. A. Poisoning the Oxygen Reduction Reaction on Carbon-Supported Fe and Cu Electrocatalysts: Evidence for Metal-Centered Activity. *J. Phys. Chem. Lett.* **2011**, 2, 295-298.
64. Liang, Y.; Li, Y.; Wang, H.; Zhou, J.; Wang, J.; Regier, T.; Dai, H. Co3O4 nanocrystals on graphene as a synergistic catalyst for oxygen reduction reaction. *Nat Mater* **2011**, 10, 780-786.
65. Liang, H.-W.; Zhuang, X.; Brüller, S.; Feng, X.; Müllen, K. Hierarchically porous carbons with optimized nitrogen doping as highly active electrocatalysts for oxygen reduction. *Nat Commun* **2014**, 5.
66. Ai, K.; Liu, Y.; Ruan, C.; Lu, L.; Lu, G. Sp2 C-Dominant N-Doped Carbon Sub-micrometer Spheres with a Tunable Size: A Versatile Platform for Highly Efficient Oxygen-Reduction Catalysts. *Adv. Mater.* **2013**, 25, 998-1003.
67. Zhang, L.; Su, Z.; Jiang, F.; Yang, L.; Qian, J.; Zhou, Y.; Li, W.; Hong, M. Highly graphitized nitrogen-doped porous carbon nanopolyhedra derived from ZIF-8 nanocrystals as efficient electrocatalysts for oxygen reduction reactions. *Nanoscale* **2014**, 6, 6590-6602.
68. Qiu, K.; Guo, Z. X. Hierarchically porous graphene sheets and graphitic carbon nitride intercalated composites for enhanced oxygen reduction reaction. *J. Mater. Chem. A* **2014**, 2, 3209-3215.
69. Geng, D.; Chen, Y.; Chen, Y.; Li, Y.; Li, R.; Sun, X.; Ye, S.; Knights, S. High oxygen-reduction activity and durability of nitrogen-doped graphene. *Energy Environ. Sci.* **2011**, 4, 760-764.
70. Chai, G. S.; Shin, I.; Yu, J. S. Synthesis of ordered, uniform, macroporous carbons with mesoporous walls templated by aggregates of polystyrene spheres and silica particles for use as catalyst supports in direct methanol fuel cells. *Adv. Mater.* **2004**, 16, 2057-2061.
71. Neburchilov, V.; Martin, J.; Wang, H.; Zhang, J. A review of polymer electrolyte membranes for direct methanol fuel cells. *J. Power Sources* **2007**, 169, 221-238.
72. Du, C. Y.; Zhao, T. S.; Xu, C. Simultaneous oxygen-reduction and methanol-oxidation reactions at the cathode of a DMFC: A model-based electrochemical impedance spectroscopy study. *J. Power Sources* **2007**, 167, 265-271.
73. Larminie, J.; Dicks, A.; McDonald, M. S. *Fuel cell systems explained*. Wiley New York: 2003; Vol. 2.
74. Büchel, G.; Unger, K. K.; Matsumoto, A.; Tsutsumi, K. A Novel Pathway for Synthesis of Submicrometer-Size Solid Core/Mesoporous Shell Silica Spheres. *Adv. Mater.* **1998**, 10, 1036-1038.
75. Kruk, M.; Jaroniec, M.; Sayari, A. Application of Large Pore MCM-41 Molecular Sieves To Improve Pore Size Analysis Using Nitrogen Adsorption Measurements. *Langmuir* **1997**, 13, 6267-6273.
76. Kruk, M.; Jaroniec, M.; Gadkaree, K. P. Nitrogen Adsorption Studies of Novel Synthetic Active Carbons. *J. Colloid Interface Sci.* **1997**, 192, 250-256.
77. Wu, Z.-Y.; Xu, X.-X.; Hu, B.-C.; Liang, H.-W.; Lin, Y.; Chen, L.-F.; Yu, S.-H. Iron Carbide Nanoparticles Encapsulated in Mesoporous Fe-N-Doped Carbon Nanofibers for Efficient Electrocatalysis. *Angew. Chem. Int. Ed.* **2015**, 8179-8183.
78. Lide, D. R. *CRC handbook of chemistry and physics*. CRC press: 2004.

79. Gasteiger, H. A.; Ross, P. N. Oxygen Reduction on Platinum Low-Index Single-Crystal Surfaces in Alkaline Solution: Rotating Ring DiskPt(hkl) Studies. *J. Phys. Chem.* **1996**, 100, 6715-6721.
80. Wu, J.; Jin, C.; Yang, Z.; Tian, J.; Yang, R. Synthesis of phosphorus-doped carbon hollow spheres as efficient metal-free electrocatalysts for oxygen reduction. *Carbon* **2015**, 82, 562-571.
81. Xing, W.; Yin, G.; Zhang, J. *Rotating Electrode Methods and Oxygen Reduction Electrocatalysts*. Elsevier: 2014.

Table of Contents

Fe-N-doped mesoporous carbon capsules were employed as an electrocatalyst for the oxygen reduction reaction (ORR). The catalysts exhibited high catalytic activity and a remarkable stability in both acid and basic media.